10/7-21-95 OSTI

SANDIA REPORT

SAND95-8235 • UC-721
Unlimited Release
Printed July 1995

Cryocycling of Energetic Materials: Status Report for FY94

S. Griffiths, J. Handrock, D. Kasberg, J. Lipkin, R. Nilson, V. Revelli, L. Weingarten, L. Whinnery

Edited by:
J. Lipkin

Prepared by
Sandia National Laboratories
Albuquerque, New Mexico 87185 and Livermore, California 94551
for the United States Department of Energy
under Contract DE-AC04-94AL85000

SAND95-8235
Unlimited Release
Printed July 1995

UC-721

CRYOCYCLING OF ENERGETIC MATERIALS: STATUS REPORT FOR FY94

J. Lipkin
Technology Applications Department

D. Kasberg
Engineering for Energy and Environment Department

L. Whinnery
Materials Synthesis & Processes Department

J. Handrock, V. Revelli, and L. Weingarten
Structural & Thermomechanical Modeling Department

S. Griffiths, and R. Nilson
Thermal & Plasma Processes Department
Sandia National Laboratories/California

Edited by

J. Lipkin
Technology Applications Department
Sandia National Laboratories/California

ABSTRACT

The Cryocycling of Energetic Materials Project is sponsored by the Memorandum of Understanding (MOU) on advanced munition technologies. This MOU is an agreement between the Department of Energy and the Department of Defense (Office of Munitions) that facilitates the development of technologies of mutual interest to the two Departments. The cryocycling project is one of several that focus on demilitarization aspects of conventional weapons and weapon systems. During FY94 the project pursued the development of analytical and numerical models that can be used to describe and optimize the cryocycling process for preparing energetic materials for recycle and reuse. In addition, the demilitarization stockpile of the Department of Defense was analyzed to identify candidate munitions for the process, and pilot scale cryocycling operations were begun at an industrial contractor.

CONTENTS

ILLUSTRATIONS

CRYOCYCLING OF ENERGETIC MATERIALS: Status Report For FY94

INTRODUCTION

Increasingly stringent environmental regulations are limiting the use of traditional methods to dispose of rocket motors and other munitions. New disposal methods are expected to make full use of the R^3 concept — Resource Recovery and Recycle — by focusing on processes that allow cost-effective reuse of the excess energetic materials in these munitions.

Propellant or explosive removal is the first step in implementing R^3 processes for solid rocket motors and munitions. Subsequent steps include size reduction and preparation of the material for recycle and reuse. Once it is suitably prepared, the processed propellants and explosives can be introduced into the feed streams of the commercial explosives industry for direct reuse. Alternatively, the high value constituents of these materials can be chemically extracted for reuse.

This project uses a systems approach to integrate key R^3 processes for excess explosives and solid propellants in the demilitarization inventories of DoD and DOE. These processes are: energetic material removal, size reduction, and feed preparation. The systems integration aspect of the project will be accomplished by developing and demonstrating a pilot scale process for environmentally conscious demilitarization of tactical rocket motors fueled with solid propellant.

Cryocycling technology contributes to such an integrated approach. When a material is cryocycled, it is repeatedly subjected to cycles of rapid cooling in a liquid nitrogen bath at 77K (-196°C) followed by warming to ambient temperature. In laboratory and pilot scale demonstrations, we have shown that cryocycling can dramatically reduce the size of a variety of propellant grains and a number of cast and plastic bonded explosives. Nevertheless, the effectiveness of this process in an integrated system that includes propellant or explosive removal must be determined. An important project goal is the fundamental understanding of the cryocycling phenomenon required to optimize such an integrated system. Achieving this goal requires modeling the cryocycling process and analyzing how material properties and processing conditions affect the process.

BACKGROUND

When they are cryocycled, energetic materials are subjected to repeated thermal cycles between ambient and liquid nitrogen temperatures. A material's thermal and mechanical properties change during this process, and the thermal gradients produce material- and geometry-dependent stresses. We observe that cracks form quickly during both the freezing and thawing portions of a cryocycle. These cracks occur because the material's ductility is substantially reduced at low temperature and internal stresses generated by thermally shocking the material exceed local strength. The size of some propellant grains and explosives are reduced by the cracking to 1-5 mm after 3-5 cycles. We conclude that cryocycling a rocket motor, for example, is thus a potentially efficient process for both removal and reducing the size of the propellant grain.

Several operational and environmental benefits accrue from using cryocycling to remove and size propellants and explosives. First, nitrogen is one of the least reactive, lowest cost, and safest chemicals known. Environmental concerns are thus minimized since the liquid nitrogen used in cryocycling does not generate a hazardous waste stream. Second, process monitoring requirements are limited. Third, recovery of the nitrogen is not necessary because it makes up approximately 80% of the atmosphere and is as easy (or easier) to obtain by condensing air than by recovering it. Fourth, a cryocycling process adds no energy and does not require moving parts in contact with the material. Safety concerns are thus minimized. A final benefit of cryocycling is that it preserves energetic properties and thus simplifies material reuse in the commercial explosives industry.

Analysis and modeling of the cryocycling process are the principal thrusts of the project. Three complementary cryocycling modeling tools are under development to characterize and simulate key process features. The first tool is an analytical model that predicts crack propagation and initiation. The second is a network model that simulates growth and interaction of numerous arbitrary fractures. The final modeling tool employs the finite element method to represent propellant geometry and process boundary conditions realistically.

The analytical model generates closed form solutions for idealized geometries. This model is limited to applications where straight cracks run perpendicular to cooled surfaces and material properties are uniform. Nevertheless, the analytical model can be used to evaluate the likelihood of cracking on first cooling as well as to estimate times for crack initiation and arrest. The smallest particle size that will fracture can also be determined from applying the analytical model.

The network model was developed prior to the initiation of this project to simulate the growth and interaction of a large number of arbitrary fractures. It has already been demonstrated that the predictions of the network model correlate well with observed fractures that develop during cryocycling experiments using inert materials.

The network model is limited, however, because it currently assumes that material properties are time- and temperature-independent. It is anticipated that this restriction will be relaxed in the near future. No results of the network modeling are included in this report.

The finite element modeling effort is currently receiving considerable attention in this project. We have developed thermal and structural finite element models for Sandia's ZUNI and HVAR rocket motor propellant grains in an effort to predict the response of these grains to pilot scale processing operations underway at Global Environmental Solutions, Inc.(GES), Magna, UT. Both grains are roughly 125 mm in diameter, 1.3 m long, and weigh 12 kg; the ZUNI has a star shaped cross section and the HVAR has a cruciform shape. These rocket motors represent a significant fraction of the Sandia inventory of excess energetic materials. The finite element models include definition of geometry and temperature-dependent material properties, and they are utilized to compute time-dependent temperature and stress fields.

In addition to the modeling and simulation studies outlined above, several other activities are underway in this project. These include an analysis of the DoD inventory of tactical rocket motors and pursuit of cooperative efforts with Lawrence Livermore National Laboratories (LLNL) and GES. The cooperative efforts are focused on applications and implementation of cryocycling for secondary explosives and for batch processing of large numbers of tactical rocket motors.

ACCOMPLISHMENTS

ANALYTICAL MODELING

The analytical model developed during the last year uses closed-form solutions to describe temperature and stress histories induced by cryocycling. These solutions illustrate the role of material properties and process parameters in determining:

- the potential of a material to fracture during cryocycling
- the time required to complete cryocycling
- the ultimate fragment size a material can achieve under cryocycling conditions.

Recent comparisons of model predictions with experimental observations are encouraging, but they also underscore the importance of having reliable data for the mechanical properties of candidate materials at liquid nitrogen temperature.

The model describes fracture initiation in a slab of thickness $2a$ that is suddenly plunged into a liquid nitrogen bath having a temperature T_b colder than the initial slab temperature T_o. The temperature distribution within the slab is given by a well known series solution that satisfies the one dimensional Cartesian conduction equation subject to a convective boundary condition of the form $-k\,dT/dx=h(T-T_b)$.[1]

$$\frac{T - T_b}{T_o - T_b} = \sum_{n=1}^{\infty} \frac{2Bi \sec \lambda_n}{Bi(1 + Bi) + \lambda_n^2} \cos(\lambda_n x^*)\, e^{-\lambda_n^2 Fo}$$

The temperature depends on the fractional distance from the center of the slab, $x^*=(x-a)/a$, the normalized time or Fourier number, $Fo=at/a^2$, and the Biot number, $Bi=ha/k$ in which k and

a are the thermal conductivity and thermal diffusivity of the solid. The series summation extends over the discrete eigenvalues, l_n, which are roots of the characteristic equation $l_n \tan l_n = Bi$.

Since many solid propellants behave elastically at moderate strains (<1%) and low temperature, the thermally induced tensile stress parallel to the cooled surface is related to the temperature distribution through the following integral equations:

$$\sigma = \phi - \frac{\bar{E}}{\bar{E}}\bar{\phi} \quad \text{where} \quad \phi = \frac{E}{1-\upsilon}\int_{T_g}^{T} \beta \, dT \quad , \quad \bar{\phi} = \frac{1}{2a}\int_0^{2a} \phi \, dx \quad , \text{and} \quad \bar{E} = \frac{1}{2a}\int_0^{2a} E \, dx \quad .$$

These are derived from the theory of elasticity[2], taking into account temperature variations in the elastic modulus E and thermal expansion coefficient b. Poisson's ratio n is assumed constant.

Time histories of T and s are generated by evaluating these expressions for sequential choices of the Fourier number, Fo. The Biot number is first determined for particular values of k, a, and the convective heat transfer coefficient, h. Since the initial propellant temperature is well above the 77K boiling point of liquid nitrogen, the convection coefficient is estimated from an analytic function [3-4] which smoothly transitions between a pair of data correlations which separately describe the film and nucleate boiling regimes. Once the Biot number is established, the temperature profile $T(x_i)$ is calculated by summing the series solution at a discrete set of points x_i. The corresponding stress profiles $s(x_i)$ are next generated by numerical quadrature.

A typical family of temperature profiles is shown in Figure 1 for a 50 mm slab of CYH. At Fo=10^{-2} the slab surface temperature has just fallen below the glass transition temperature of CYH (225K). Thereafter, in the time window between Fo=3×10^{-2} and 10^{-1}, the transition from film to nucleate boiling occurs, causing a considerable increase in the heat transfer coefficient and a corresponding reduction of the surface temperature. By Fo=1, the slab temperature is nearly uniform and in equilibrium with the liquid nitrogen bath.

The corresponding stress distributions presented in Figure 2 are strongly influenced by the thousand-fold increase in elastic modulus that occurs as the material passes through its glass transition. Prior to Fo=10^{-2}, nearly all of the material remains warmer than the transition temperature, T_g. For that time, the propellant's modulus is so small that thermally induced stresses are negligible. As cooling proceeds beyond Fo=10^{-2}, the glass transition front sweeps inward from the surface to the interior. By Fo=10^{-1}, the outer 40% of the slab has been cooled below T_g, as apparent in the stress profiles which indicate significant stresses over the interval $0<x/a<0.4$. It is apparent from these results that surface tensile stresses are balanced by internal compressive stresses, and that this balance must be maintained entirely within the high-modulus material. This restriction on the stresses in the thermally influenced region reduces the maximum tensile stresses to less than 1/4 of the maximum attainable stress, $s_0=f(T_b)$, which is used as a reference stress in scaling the vertical axis of Figure 2.

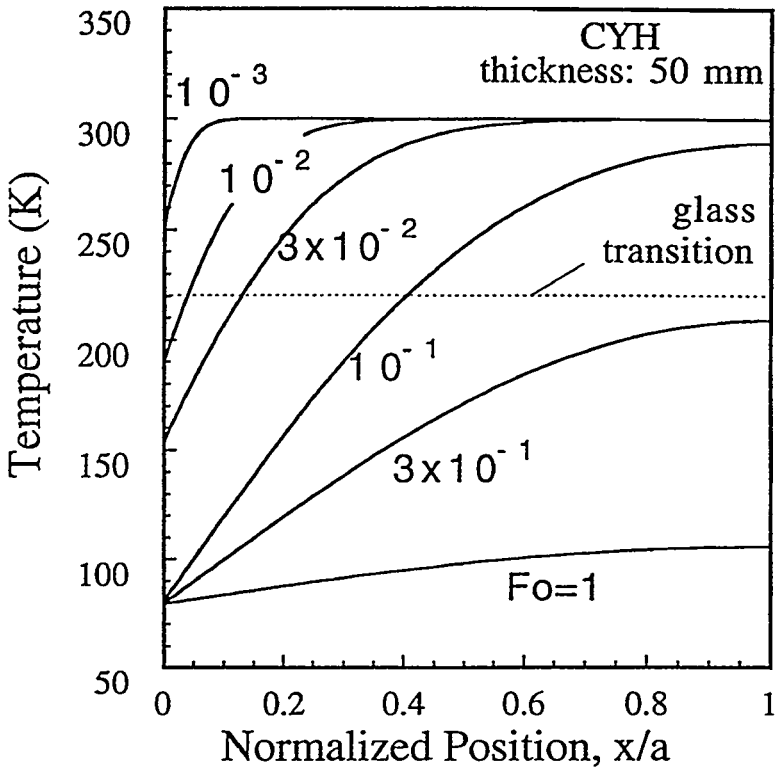

Figure 1. Predicted temperature profiles in a 50 mm slab of CYH.

Figure 2 illustrates two important aspects of cryocycling that are generally valid regardless of process parameters. First, the maximum stress occurs in a time range from Fo=1-3x10^{-1}, a time much shorter than the thermal equilibration time of Fo=1.0.

Cooling beyond Fo=3x10^{-1} thus provides little added benefit and needlessly extends both the cooling and warming phases of the cycle. The second general observation is that stresses always remain compressive in the central region of the slab, indicating that the fractures produced on cooling cannot penetrate more than about 50-70% of the distance from the surface to the center. It is, however, possible to extend fractures through the center of the slab by subsequently heating the exterior, thereby producing compressive stresses at the surface and tensile stresses in the interior. Accordingly, sequential cycles of rapid cooling and heating should be particularly effective in breaking a material.

We can predict the occurrence of fractures in the material by comparing the local, time-dependent stress at the surface with the temperature-dependent strength at the same location. Before stresses become significant, the strength of the surface material typically increases by about one order of magnitude during the glass transition. Thereafter, the ratio of stress to strength grows for a while, reaches a maximum, and then subsides as temperatures equilibrate and stresses diminish.

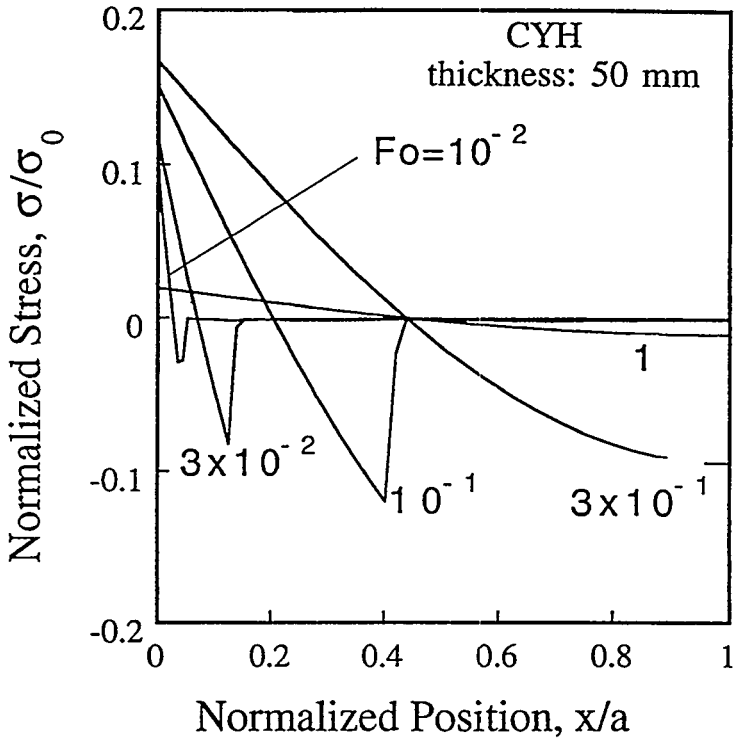

Figure 2. Predicted stress profiles in a 50 mm slab of CYH.

Figure 3 displays the calculated maximum ratio of stress to strength for five propellants, two propellant simulants (LWCYH and H19), a plastic bonded explosive (PBX), as well as for the polystyrene (POLY) that was used in cryocycling experiments. The order from left to right is based on the experimental ranking of "best" to "worst" susceptibility to cryocycling. Three broad categories of propellants are represented by the results for specific propellants shown in Figure 3. Double base formulations are represented by N5, composite propellants are represented by QDT, and composite modified double base propellants are represented by CYH and EJC.

The calculated ratio of stress to strength is clearly greatest at the left, falling gradually to the right, in keeping with the experimental ranking. The ratio of stress to strength is greater than unity for all materials (except H19), indicating that a 25 mm slab of any one (except H19) should fracture.

The minimum fragment size obtainable by cryocycling can be estimated by calculating the maximum ratio of stress to strength as the slab thickness becomes successively smaller. As the thickness decreases, heat conduction becomes more effective in reducing the temperature difference and, hence, thermal stress within the slab. The minimum fragment sizes shown in Figure 4 are the slab thicknesses which resulted in a unit ratio of stress to strength. Presumably a slightly thicker slab would break in two, while a slightly thinner slab would remain in one piece.

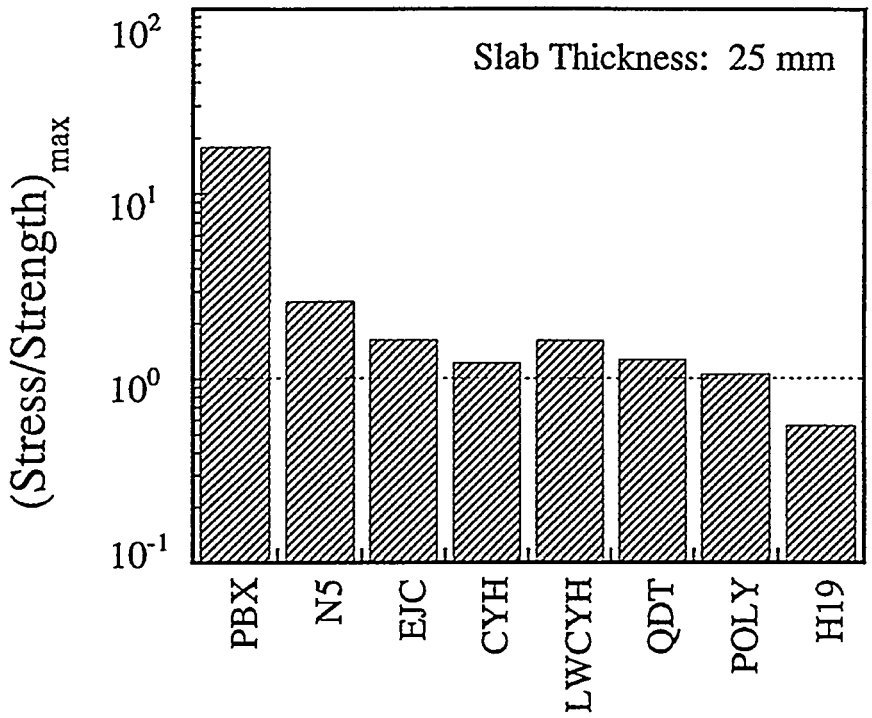

Figure 3. Maximum ratio of stress to strength; comparison of predictions (bar height) with experimental observations (horizontal ranking).

So the minimum particle size should be as displayed in Figure 4 or, perhaps, one half that large. The smallest sizes are predicted for the leftmost materials that were, in fact, deemed "best" in cryocycling experiments because they yielded the smallest fragment sizes.

The predicted fragment sizes shown in Figure 4 agree reasonably well with those observed experimentally. For example, cryocycling of H19 resulted in an average particle size of 60 mm, in remarkable agreement with predictions. In the middle of the spectrum, LWCYH broke down to an average particle size of roughly 8 mm, as compared with a prediction of 6 mm; QDT and EJC produced similar particle sizes, in general agreement with the model. Cryocycling of PBX produced many small fragments (< 5mm) which were themselves severely cracked and so friable that the ultimate particle size was expected to be less than 1 mm. Indeed, the predictions suggest that a considerably smaller size (0.2 mm) would be obtained if the material behaved as a continuum at length scales of less than 1 mm.

While these comparisons of analytical and experimental results are generally encouraging, they nevertheless illustrate the importance of obtaining reliable measurements of strength and modulus, especially at liquid nitrogen temperature. For example, a 50% uncertainty in either of these quantities can result in an order of magnitude uncertainty in predicting the

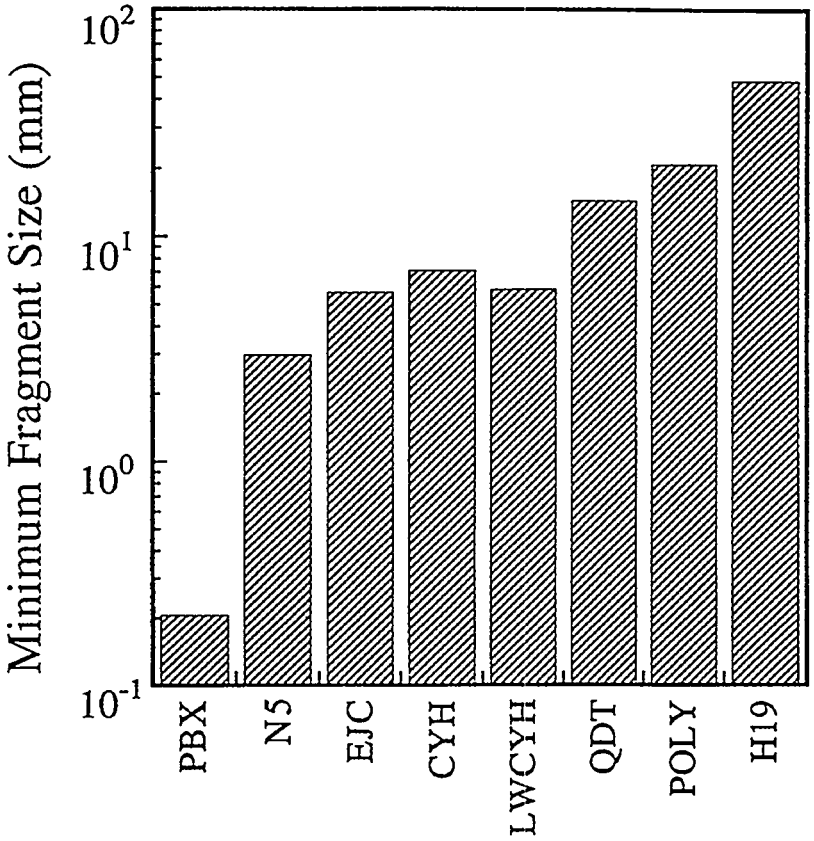

Figure 4. Minimum particle size obtainable by cryocycling; comparison of predictions (bar height) with experimental observations (horizontal ranking).

ultimate particle size since the maximum attainable stress rarely exceeds the cryogenic strength by more than 50% to 100%. Among the materials considered here, polystyrene and PBX are probably the best characterized, since they experience glass transition above or near room temperature. The properties of QDT and EJC were carefully measured by Hercules, Inc. at liquid nitrogen temperature but are lacking at intermediate temperatures. Conversely, the temperature dependence is known for CYH and N5 from 173 to 300K, but the low temperature behavior must be extrapolated. Finally, although the properties of the inert propellant simulants, LWCYH and H19, were measured over the full temperature range, the two different experimental techniques used in these measurements produced different values for the low temperature modulus; we chose to use the larger values for the sake of consistency with other materials.

FINITE ELEMENT SIMULATIONS

The overriding goal of the finite element analysis activity in this project is predicting the thermostructural response of rocket motor propellants and explosives during the first cryocycle.

In the current year, our analysis efforts concentrated on the cooling portion of the process, i.e., after the energetic material is submerged in liquid nitrogen. In the future, the warm-up portion of the cycle will be simulated using the same techniques. Present and future results address the effects of cycle time, case constraints, propellant configuration, and liquid nitrogen contact surfaces on propellant response. As described in this report, a procedure has been implemented whereby crack initiation and propagation in the propellant are simulated during the first cryocycle. In addition, in situations where the propellant or explosive is bonded to a case, we have predicted and simulated bond line failures that may occur during the process.

Code Selection

Several criteria were considered in selecting the finite element code used in this effort. A key criterion was that the thermal and structural analyses should be completed using either a single code or two codes allowing straightforward transfer of thermal output to the structural analysis. In addition, an effort was made to use existing technology wherever possible so that development of new fracture models and numerical implementations were not necessary. A number of codes available to analysts were surveyed. Ultimately, the ABAQUS code[5] was selected since it best satisfied problem constraints. ABAQUS allows easy movement of results from a thermal to a structural analysis with the same mesh discretization. In this application, a relatively sophisticated temperature-dependent film coefficient was necessary in the analyses. A user subroutine was developed to implement this aspect of the simulation. The code also contains a failure model which has potential applications in the current problem.

Model Development

Thermal and structural finite element models were developed for Sandia's ZUNI and HVAR propellant grains. These rocket motors represent a significant fraction of the Sandia inventory and are currently being used by GES as test units for developing prototype cryocycling processes.

The PATRAN 3.0 pre-processor[6] was used to generate models of the cross section of the rocket motors. Two-dimensional models were formulated assuming the cross section is primarily in plane strain (no end effects). Symmetry conditions of the motor cross sections were used to reduce computational time. That is, a sixteenth section of the ZUNI and an eighth section of the HVAR were modeled. PATRAN produced an ABAQUS input file which was edited to include temperature-dependent material properties, a boiling heat transfer coefficient, and selection of time-dependent bounds on solution incrementation.

The ZUNI and HVAR propellants were Standard X-8 and JPN, respectively. Due to the lack of documented temperature-dependent properties on these propellants, a single material data set was developed based upon a combination of these properties and those available for N5. The N5 propellant has a formulation which is similar to X-8 and JPN, providing justification for using the considerable database of temperature-dependent N5 material properties[7-9]. The properties used in these analyses were density, conductivity, specific heat, uni-axial stress-strain relation, and coefficient of thermal expansion. An example of the extracted data is the stress-strain response shown in Figure 5.

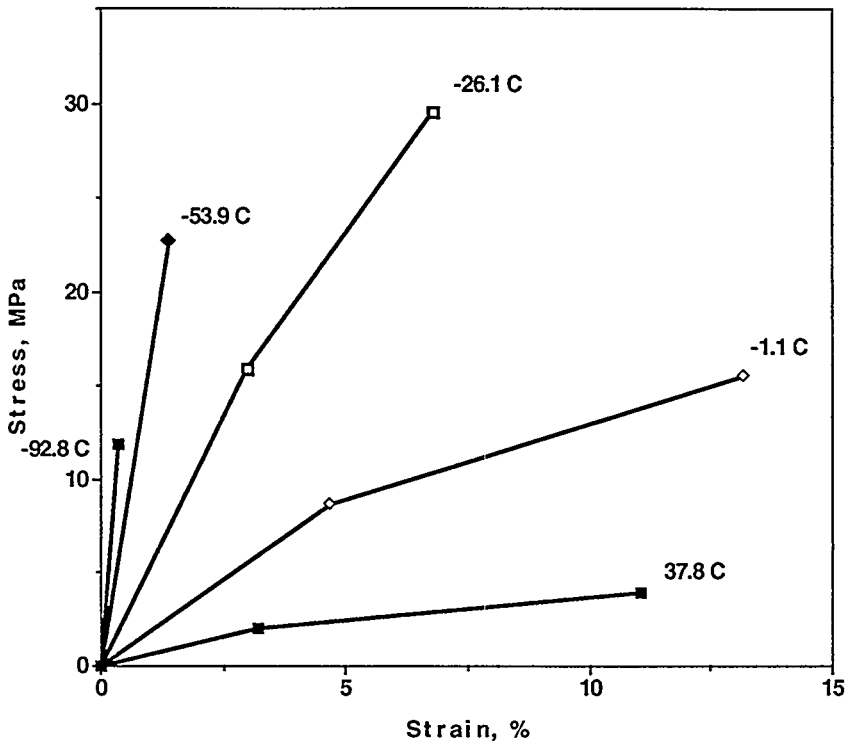

Figure 5. Propellant uniaxial stress vs strain curves used in finite element calculations.

A mathematical relationship for the boiling heat transfer coefficient between liquid nitrogen and the model surfaces was obtained from References 3 and 4. A plot of this relationship is shown in Figure 6. A subroutine describing this behavior was written and linked into the ABAQUS code. The analyses start at room temperature (25°C), corresponding to a temperature difference of 221°C with the liquid nitrogen. Surfaces in contact with the liquid nitrogen thus start out near the right end of the curve in Figure 6. As the propellant temperature approaches that of the liquid nitrogen, one moves to the left on the curve. At a temperature difference of approximately 30°C, the coefficient increases about 2 orders of magnitude over a relatively small temperature change. This behavior is followed by a change in slope. Such rapid variations cause convergence difficulties in the finite element code. These difficulties were resolved by selecting appropriate incrementation parameters.

Results

As noted earlier, analyses were performed on the ZUNI and HVAR propellant configurations. Since the propellant can be removed in its entirety from these rocket motors, our analyses assume liquid nitrogen is in contact with all external propellant surfaces. A thermal gradient moves through the propellant as it cools. This thermal gradient generates stress fields

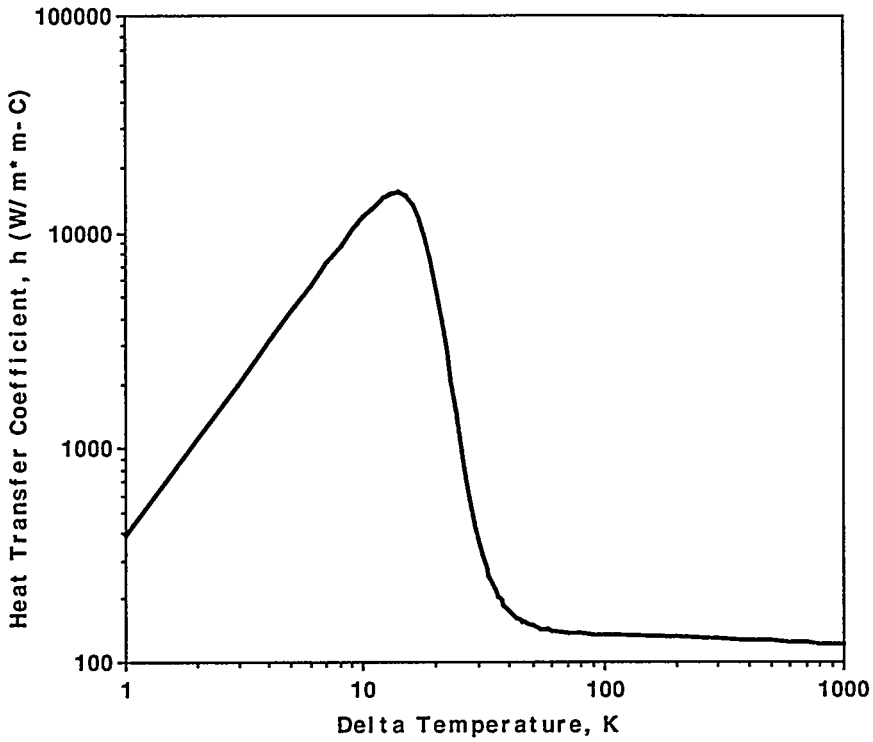

Figure 6. Liquid nitrogen boiling heat transfer coefficient.

which can lead to cracking. Two snapshots in time of the temperature and stress distributions of the ZUNI propellant are shown in Figure 7. The analyses that produced these results did not include a propellant cracking model. At this stage, the emphasis was to demonstrate thermostructural modeling capabilities.

For the next step in the analysis, a capability was developed for numerically simulating propellant cracking and case debonding. The ABAQUS code allows debonding surfaces between elements based upon the normal and shear strengths of the material. If elements separate based upon this strength criterion, the element faces can move relative to each other. This movement includes separation, sliding, and subsequent re-contact. Ultimately, we are aiming for a global cracking model which allows debonding (cracking) between all elements in the propellant and between the propellant and the case. As a first step in developing such a model, several possible debonding locations were placed within a "case-bonded" ZUNI propellant finite element mesh. That is, the ZUNI propellant grain model was used, and a fictitious aluminum case 3.5 mm thick was attached with an infinitesimal bond line. The assumed debonding locations were along a symmetry plane, emanating from a free surface, and intersecting within the propellant. In addition, the technique was used to model debonding between the propellant and the case. The locations of possible debonding interfaces for this initial study are shown by the heavy black lines in the upper left graphic of Figure 8. The remaining three graphics of Figure 8 depict crack formation as a function of time. The first cracks that are formed occur at the propellant to liquid nitrogen interface. As time progresses

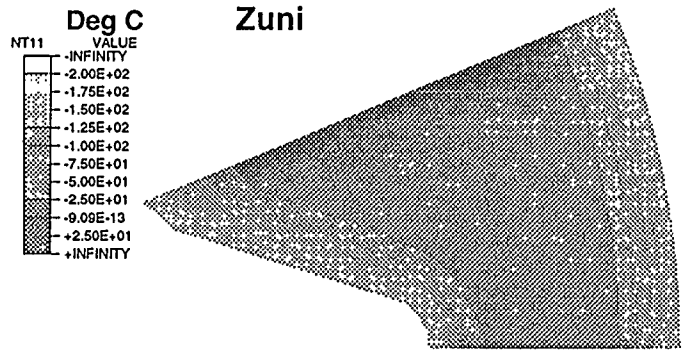

Temperature Distribution at 1 Minute

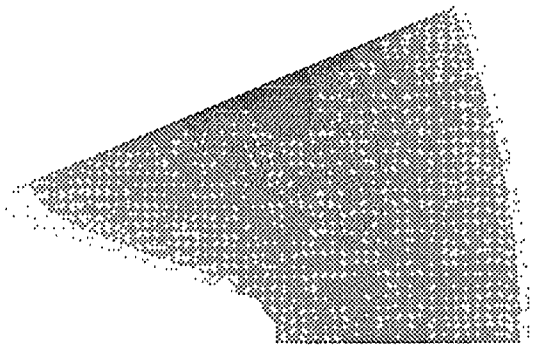

Temperature Distribution at 5 Minutes

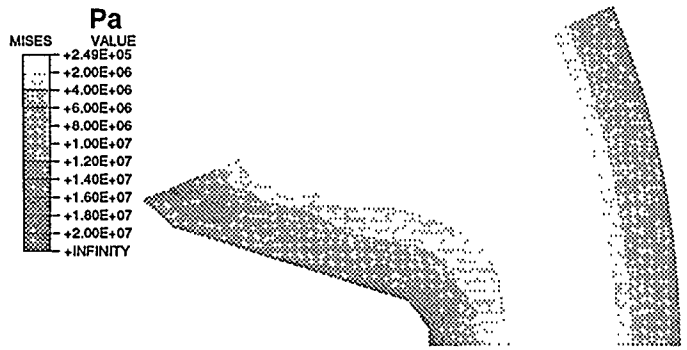

von Mises Stress Distribution at 1 Minute

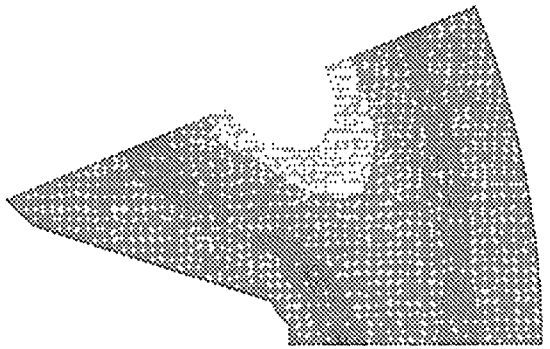

von Mises Stress Distribution at 5 Minutes

Figure 7. Temperature and stress distributions in ZUNI propellant grain during first cooling cycle.

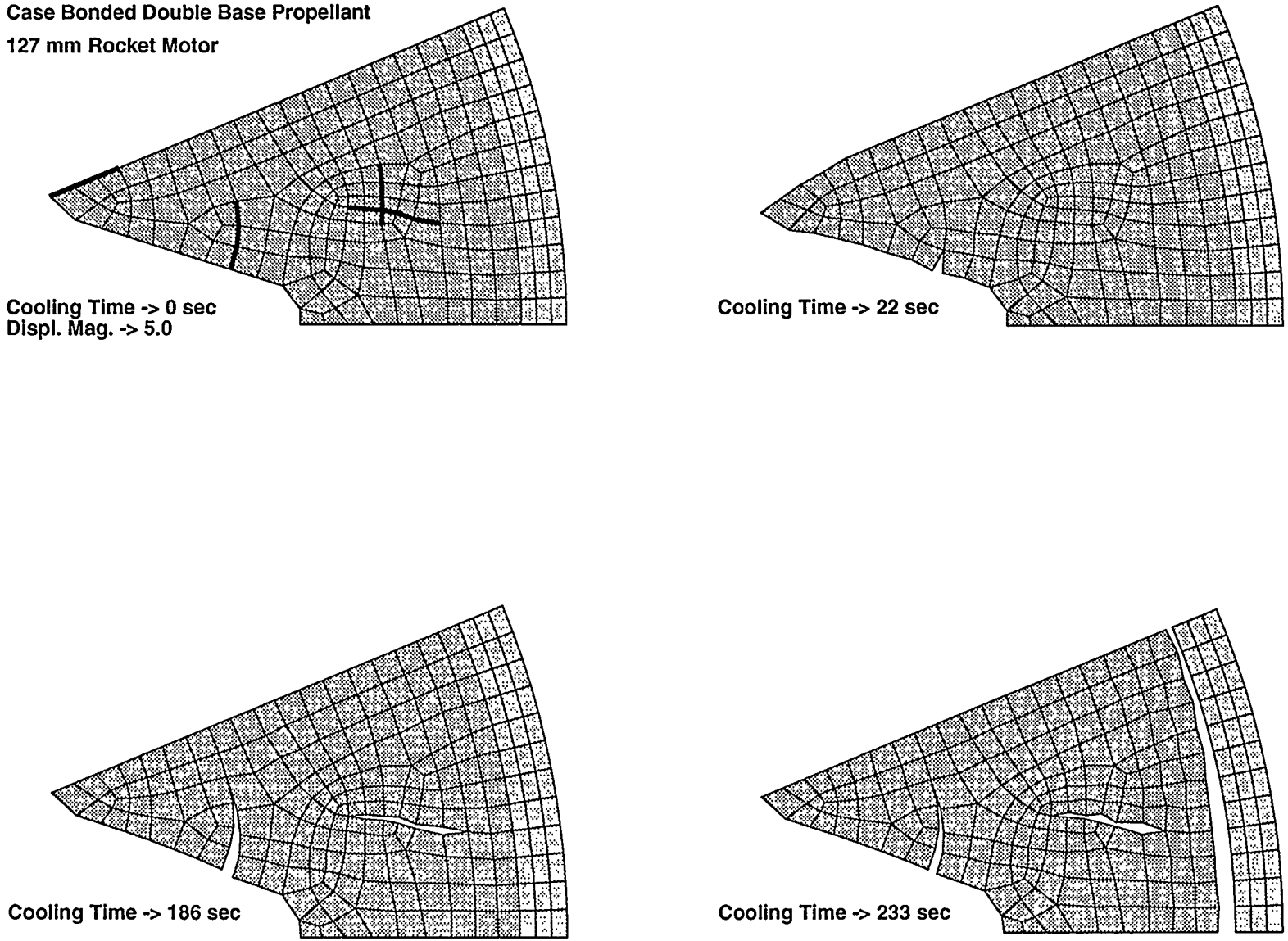

Figure 8. Cracking and debonding simulations for case bonded, double based propellant grain.

and the thermal gradient proceeds into the propellant, additional surfaces debond (crack) at interior locations. In addition, the propellant and case eventually debond. These results provide confidence that implementation of a global cracking model is feasible.

ANALYSIS OF DoD DEMILITARIZATION INVENTORY

An analysis of the DoD Resource Recovery and Disposition Account (RRDA) is being performed to assess the impact cryocycling will have on demilitarization of the DoD tactical rocket motor inventory. The analysis will also aid in downselecting candidate tactical rocket motors for demonstrations of cryocycling as an energetic material removal and size reduction process. Munitions placed in the RRDA by the military services are compiled in a handbook known as the Orange Book. Items in the Orange Book are available for resource recovery to other organizations or are identified for demilitarization and disposal. This section discusses the current status of our analysis of the Orange Book.

Requirements for the Orange Book analysis are:

- identify items fitting the tactical rocket motor category
- identify items representing a significant fraction of the demilitarization inventory in the Orange Book
- match the cryocycling technology to the identified items.

The Orange Book lists over 16,300 individual lots of munitions stored in various quantities at military installations around the nation. Because of the extensive nature of this list, it was necessary to create a special database from an electronic copy of the Orange Book to facilitate the identification of rocket motors that are of special interest to this project. It was also necessary to contact other agencies to acquire information concerning these motors that is otherwise not available in the Orange Book, such as the chemical composition of the propellant. Information from the Orange Book database and from other sources was then compiled in a database that we can use to determine the suitability of the listed rocket motors for cryocycling processes.

The categories of information, shown in Table 1, are the basis for the Orange Book analysis.

TABLE 1

Principal Data	Storage Data	Propellant Data
Motor Type / Model	Location	Designation
Stock Number	Lot Quantity	Type
Length	Total Weight Stored	Composition
Diameter	Condition Code	Method of Manufacture
Weight		Grain Length
Case Material		Grain Diameter
Case Thickness		Grain Weight

The following agencies have been instrumental in supplying information for this effort through correspondence and private communication:

- Chemical Propulsion Information Agency (CPIA)
- U. S. Army Defense Ammunition Center and School (USADACS)
- U. S. Army Armament, Munitions and Chemical Command (AMCCOM).

The CPIA is an information analysis center for the DoD. The center maintains manuals for rocket motors and rocket motor propellants. These manuals provide detailed information on specific items on individual data sheets. The Demil Technology Office of USADACS is responsible for the data collection, compilation, and publication of the Orange Book. AMCCOM is the demilitarization center for the military services and maintains an accounting of the items designated for demilitarization at the various military storage installations.

This effort is being performed with the understanding that the quarterly publication of the Orange Book used for the analysis (March 1994) may not accurately reflect current inventory because the RRDA is extremely dynamic. However, the analysis still provides an understanding of the applicability of the cryocycling technology to the DoD demilitarization inventory. Although many other items such as projectiles and warheads contain solid propellants and explosives, the focus of this analysis is on rocket motors because the principal thrust of this project is to develop and demonstrate the cryocycling process for demilitarization of tactical rocket motors.

The combined storage weight of all items in the Orange Book is approximately 390,000 tons. These items are grouped as lots containing one munition type. There are 386 lots of rocket motors stored at various installations with a combined storage weight of 7,500 tons. It should be noted that these weight values represent rocket motor weights in the stored configuration which may include its storage container. The 386 lots represent 2% of the total weight in the RRDA, which is a significant fraction considering that the percentage would be higher if non-demilitarized motors were subtracted from the inventory, such as those recovered by other organizations or destroyed.

Since cryocycling is most efficiently applied in a batch processing mode, it is likely that this demilitarization method will be especially useful at DoD sites where significant numbers of rocket motors are stored. For this reason, our analysis was limited to lot quantities representing 100,000 pounds or more. Using this criterion, 23 lots of motors, totaling over 150,900 motors, were identified at nine different locations. These 23 lots have a combined storage weight of approximately 6,800 tons and represent 91% of the total rocket motor weight in the Orange Book.

A detailed database of the 23 lots has been generated to study the suitability of the rocket motors for the cryocycling technology. A summary of the information in the database is shown in Table 2. Fourteen different types of rocket motors are included in the 23 lots (some of the lots are the same motor type stored at different locations). The motor propellant grains range in diameter from 0.8" to 28.7" and range in weight from 1.2 lbs. to 2,160 lbs. The fourteen motor types have twelve different propellant compositions. Six of the motor types have case-bonded

TABLE 2
DoD ROCKET MOTOR DEMILITARIZATION INVENTORY *

Rocket Motor					Grain Features			
Nomenclature	Storage Location	Lot Quantity	Total Motor Weight Stored (lbs.)	Total Propellant Weight (lbs.)	Diameter x Length (in.)	Weight (lbs.)	Manufacturing Method	Type Designation
5.0 MK10-7	Red River	31,755	3,810,600	762,120	4.5 x 39.3	24.0	Cartridge loaded	JPN
5.0 MK10-7	Anniston	16,485	1,978,200	395,640	4.5 x 39.3	24.0	Cartridge loaded	JPN
5.0 MK10-6	Hawthorne	14,682	1,761,840	352,368	4.5 x 39.3	24.0	Cartridge loaded	JPN
5.0 MK10-7	Tooele	6,367	764,040	152,808	4.5 x 39.3	24.0	Cartridge loaded	JPN
5.0 MK10-7	Sierra	894	107,280	21,456	4.5 x 39.3	24.0	Cartridge loaded	JPN
5.0 MK10 MOD 5	Hawthorne	1,352	162,240	32,448	4.5 x 39.3	24.0	Cartridge loaded	JPN
M42A1 MIM	Letterkenny	664	1,082,320	498,000	16.0 x 102.0	750.0	Cartridge loaded	OIO
M42 MIM 14A	Letterkenny	272	443,360	204,000	16.0 x 102.0	750.0	Cartridge loaded	OIO
JATO MK25 MOD1	Crane	407	102,654	49,654	8.7 x 40.4	122.0	Case bonded	RDS-135
JATO	McAlester	2,254	568,509	274,988	8.7 x 40.4	122.0	Case bonded	RDS-135
XM22E8	Red River	297	324,027	179,388	13.5 x 83.0	604.0	Case bonded	ANP-2830B1 ANP-2832H0
M30	Sierra	68	261,392	146,880	28.7 x 81.7	2160.0	Case bonded	TP-E-8082
MK16 MOD 5	Hawthorne	37,696	753,920	TBD**	2.5 x 26.3	TBD	Cartridge loaded	JPN
762MM M3A2	Blue Grass	34	203,048	69,700	21.4 x 148.0	2050.0	Cartridge loaded	OIO
MK 6-3	Crane	169	174,070	11,830	7.5 x 35.7	70.0	Cartridge loaded	AN-579Y
MK 6 MOD 1	Crane	959	167,825	69,048	9.7 x 26.5	72.0	Cartridge loaded	AN-583AF
MK 6 MOD 1	McAlester	724	126,700	52,128	9.7 x 26.5	72.0	Cartridge loaded	AN-583AF
MK8-2	Tooele	572	160,160	59,202	10.6 x 26.4	103.5	Cartridge loaded	OIY
MK8-1	Hawthorne	242	110,473	25,047	10.6 x 26.4	103.5	Cartridge loaded	OIY
TOW M114	Anniston	19,820	149,751	23,784	0.8 x 13.8	1.2	Cartridge loaded	M7
MK52 MOD 2	McAlester	397	105,205	38,112	7.8 x 41.3	96.0	Case bonded	ANB-3109
2.75 SR 105J1	Sierra	11,348	238,308	94,188	2.7 x 19.0	8.3	Case bonded	ANB-3141-1
2.75 APERS	Sierra	3,518	111,697	20,756	2.7 x 19.0	5.9	Case bonded	N-5

* Stored weight > 100,000 lbs
** To be Determined

grains and eight are cartridge-loaded. The total propellant weight included in the fourteen motor types is approximately 3,630,000 pounds.

The propellant composition and manufacturing method are of interest because the first application of cryocycling as part of a demilitarization process will be greatly simplified if we use propellant grains obtained from cartridge-loaded motors. Subsequent efforts will address the more complex issues related to removing propellant from case-bonded motors. Of the 150,976 motors in the 23 lots, only 18,051 motors are case-bonded.

RECENT LABORATORY AND FIELD RESULTS

The original laboratory and field studies of cryocycling focused on inert simulants and small samples of live, solid propellants. We have significantly expanded the empirical database developed from these early studies in the last year. This database now includes:

- field demonstrations using propellant grains from full-size tactical rocket motors
- laboratory experiments on a variety of secondary high explosives.

Results from these activities are briefly reviewed in this section.

As described above, GES, a subsidiary of Hercules, Inc., is actively developing techniques to use cryocycling as part of a demilitarization process for tactical rocket motors. GES demonstrated the safety, simplicity, and effectiveness of cryocycling operations in FY94 by using individual HVAR and ZUNI motors. Generally, they observed that the propellant grain from the ZUNI motor could be cryocycled more efficiently than that from the HVAR motor; even though the two grains have quite similar compositions and weights. Finite element analyses revealed that this observation is due to differences in grain geometries for the two motors which, in turn, affect rates of cooling and warm-up. This example demonstrates that the finite element analysis is capable of capturing key aspects of the cryocycling phenomenon that are essential for optimizing any proposed process. The optimized process will produce the maximum number of fragments in the shortest time.

The evolution of particle sizes during six cryocycles of a ZUNI propellant grain are shown in Figure 9. It is evident in Figure 9 that the particle size distribution for this propellant is well established after 5-6 cryocycles, where we find most of the grain is reduced to the size range of 6 to 12 mm. Although some smaller "fines" are also observed, they make up a very small percentage of the total weight of processed material. The results in Figure 9 are encouraging because they indicate that the double base, X-8, propellant in the ZUNI motor can be effectively converted to a pulverized material in a size range that is desirable for reuse applications, such as those in the mining/blasting industries.

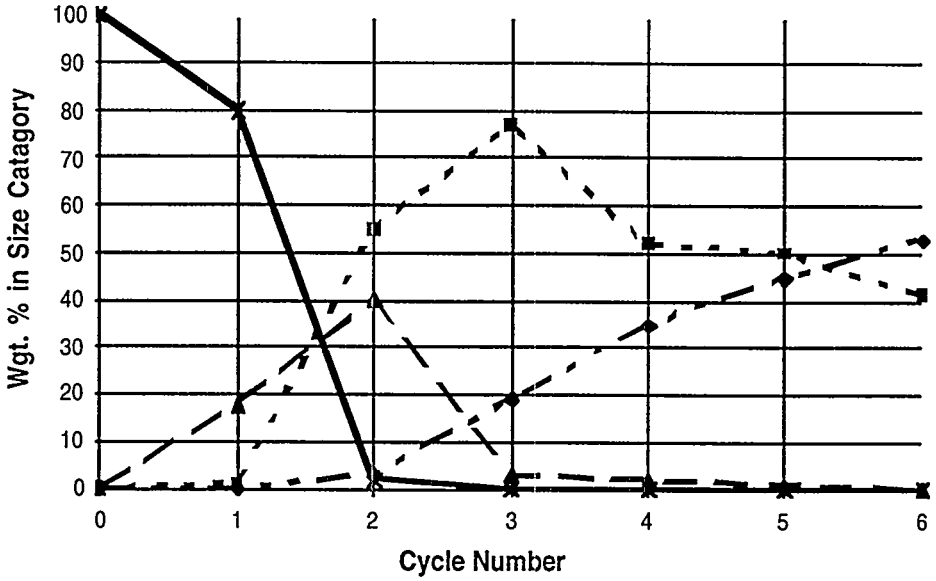

Figure 9. Cryocycling results for ZUNI rocket motor propellant.

A number of bench-scale, laboratory experiments were also carried out to assess the applicability of cryocycling to several secondary high explosives. In particular, the U.S. Army MICOM, Huntsville, AL, reported very good results for cryocycling TNT-based, melt-cast explosives such as Comp B and Octal [10]. In addition, we are working with LLNL to examine the cryocycling of LX-17, an insensitive high explosive and PBX 9404, a plastic bonded explosive. Both of these explosives are molded, pressed, and machined, if necessary, to fabricate individual components. Since their constituents are not water soluble, it was decided to enhance the cryocycling of these explosives by immersing test samples in warm water at 333K (60°C) immediately after they were removed from the liquid nitrogen bath. An internal review committee at LLNL examined proposed cryocycling procedures for these materials prior to their use in experiments. The tests of LX-17 revealed that this material is relatively difficult to cryocycle, but that it does ultimately break up into fragments of 8 mm or smaller after about 15 cryocycles. This behavior is consistent with LX-17's high toughness derived from its Kel-F binder. In contrast, samples of PBX 9404 cryocycled easily into fragments on the order of 1 mm or less in 5-6 cryocycles. This response of PBX 9404 to cryocycling was predicted prior to the tests, and is discussed in the analytical modeling section. Our experiments with secondary high explosives reveal that they can be cryocycled safely with results that depend to a large extent on the properties of the explosive. This dependence is consistent with our understanding of the key aspects of the cryocycling phenomenon.

FUTURE WORK

The development, refinement, and further applications of the analytical model will include the following:

- expanding comparisons with experimental data;
- comparing analytical model results with those from finite element analyses;
- quantifying geometric effects by comparing results for slabs and spheres;
- exploring how the warming phase of a cryocycle affects fragmentation process;
- predicting fracture spacing and, hence, number of fragments per cryocycle;
- formulating simple scaling laws that predict fragment number and size; and
- reducing the effects of uncertainty in the material property data base.

In addition, the finite element analysis and modeling efforts will focus on the following areas:

- reviewing additional material property data;
- refining cracking damage model parameters;
- implementing global propellant cracking and case debonding simulations;
- investigating grain cracking in cartridge loaded and case bonded rocket motors;
- characterizing debonding behavior in case bonded rocket motors;
- optimizing cracking response on the first cryocycle; and
- comparing finite element model calculations to analytical model results.

Analysis of the DoD demilitarization inventory will also continue. The additional information needed to develop a complete and comprehensive database of excess tactical rocket motors that are potential candidates for the cryocycling process will be acquired through contacts in the DoD and industry.

The upcoming experimental and process demonstration activities will focus on demonstrating batch processing of HVAR and ZUNI propellant grains. We will continue to work with GES by combining their expertise in handling rocket motors and solid propellants with our experience in cryocycling technology. In addition, the cryocycled propellant product will be evaluated for reuse in the commercial mining and specialty explosives industries.

REFERENCES

1. H. S. Carslaw and J. C. Jaeger, Conduction of Heat in Solids, Oxford University Press, 1976.

2. B. A. Boley and J. H. Weiner, Theory of Thermal Stresses, John Wiley, 1960.

3. Haselden, G. G. (ed.), Cryogenic Fundamentals, Academic Press, London, 1971. Chapter 3 "Heat Transfer", Clark, J. A. and Thorogood, R. M.

4. Larson, R. S., Memo to Distribution, "Calculation of Thermal Stress Profiles During Cryocycling", January 17, 1994.

5. ABAQUS, Version 5.3, HKS, Inc., Pawtucket, RI.

6. PATRAN 3.0, P3/PATRAN User Manual, PDA Engineering, Casta Mesa, CA.

7. CPIA/M2, Unit 1121, May 1968.

8. SPIA/M2g, Unit 9, December 1954.

9. Defense Technical Information Center - Reports, January 1970, May 1972, December 1979.

10. Private communication with Dr. W. S. Melvin, Propulsion Directorate, Army Missile Command (MICOM), Redstone Arsenal, Huntsville, AL.

UNLIMITED RELEASE

INITIAL DISTRIBUTION

University of California
Lawrence Livermore National Laboratories
Attn: César Pruneda, L-282
Ravi Upadhye, L-282
Bruce Watkins, L-282
7000 East Ave.
P.O. Box 808
Livermore, CA 94550

Armstrong Laboratory
Attn: Jim Hurley (AL-EQS)
139 Barnes Dr., Suite 2
Tyndall AFB, FL 32403

US Army MICOM
Propulsion Directorate
Attn: Bill Melvin
Redstone Arsenal, Alabama 35898-5249

Thiokol Corporation
Attn: Lou Cannizzo, MS 244
Bill Munson, MS 300
Brigham City, Utah 84302

TPL, Inc.
Attn: Hap Stoller
3768 Hawkins St. NE
Albuquerque, NM 87109

Global Environmental Solutions, Inc.
Attn: Kevin Farnsworth, MS X1D1
Clark de Nevers, MS X1D1
Pat Oyler, MS X1D1
4100 South 8400 West
Annex 16
Magna, Utah 84044-0098

MS 0861	W. K. Tucker, 9121
MS 9001	J. C. Crawford, 8000
MS 9002	Attn: P. N. Smith, 8500
MS 9003	D. L. Crawford, 8900
MS 9037	R. J. Detry, 8200
MS 9054	W. J. McLean, 8300

MS 9105	L. A. Hiles, 8400
MS 9141	T. M. Dyer, 8800
MS 9901	L. A. West, 8600
MS 9004	M. John, 8100
MS 9042	R. J. Kee, 8745
MS 9042	R. Nilson, 8745
MS 9042	R. S. Larson, 8745
MS 9042	S. K. Griffiths, 8745
MS 9043	J. Handrock, 8742
MS 9043	L. Weingarten, 8742
MS 9043	M. L. Callabresi, 8743
MS 9043	P. Nielan, 8742
MS 9043	V. Revelli, 8742
MS 9055	R. Behrens, 8353
MS 9101	W. Peila, 8411
MS 9101	D. Kasberg, 8411
MS 9401	R. C. Wayne, 8700
MS 9402	G. J. Thomas, 8715
MS 9404	J. Hruby, 8716
MS 9404	L. Whinnery, 8716 (5)
MS 9405	D. L. Lindner, 5404
MS 9410	J. C. Swearengen, 8113 (5)
MS 9410	J. Lipkin, 8113 (10)

MS 9021	Technical Communications Department 8535, for OSTI (10)
MS 9021	Technical Communications Department 8535/Technical Library, MS0899, 13414
MS 0899	Technical Library Department, 13414 (4)
MS 9018	Central Technical Files, 8523-2 (3)